International Journal of Thermophysics, Vol. 21, No. 6, 2000

Molar Heat Capacity at Constant Volume of Trifluoromethane (R23) from the Triple-Point Temperature to 342 K at Pressures to 33 MPa

J. W. Magee[1, 2] and H. A. Duarte-Garza[1, 3]

Received May 22, 2000

Molar heat capacities at constant volume (C_v) of trifluoromethane (R23) have been measured with an adiabatic calorimeter. Temperatures ranged from the triple point to 342 K, and pressures up to 33.5 MPa. Measurements were conducted on the liquid in equilibrium with its vapor and on compressed liquid and gaseous samples. The samples were of high purity, as verified by chemical analysis. Calorimetric quantities are reported for the two-phase ($C_v^{(2)}$), saturated-liquid (C_σ or C'_x), and single-phase (C_v) molar heat capacities. The $C_v^{(2)}$ data were used to estimate vapor pressures for values less than 100 kPa by applying a thermodynamic relationship between the two-phase internal energy $U^{(2)}$ and the temperature derivatives of the vapor pressure. The triple-point temperature and the enthalpy of fusion were also measured. The principal sources of uncertainty are the temperature rise measurement and the change-of-volume work adjustment. The expanded relative uncertainty (with a coverage factor $k = 2$ and thus a two-standard deviation estimate) is estimated to be 0.7% for C_v, 0.5% for $C_v^{(2)}$, and 0.7% for C_σ.

KEY WORDS: enthalpy of fusion; heat capacity; trifluoromethane; triple point; R23; vapor pressure.

1. INTRODUCTION

Thermodynamic properties of a fluid may be calculated from a knowledge of its ideal-gas properties and an accurate equation of state. Heat capacities

[1] Physical and Chemical Properties Division, Chemical Science and Technology Laboratory, National Institute of Standards and Technology, Boulder, Colorado 80305, U.S.A.
[2] To whom correspondence should be addressed. E-mail: joe.magee@nist.gov.
[3] Present address: Union Carbide, P.O. Box 8361, Building 740-3105, 3200 Kanawha Turnpike, South Charleston, West Virginia 25303-8361, U.S.A.

0195-928X/00/1100-1351$18.00/0

derived in this manner, however, often lack sufficient accuracy since the calculation involves integration of the isochoric curvature $(\partial^2 p/\partial T^2)_\rho$ as in the equation

$$C_v - C_v^o = -T \int_0^\rho \left(\frac{\partial^2 p}{\partial T^2} \right)_\rho \frac{d\rho}{\rho^2} \tag{1}$$

where C_v^o is the ideal-gas heat capacity. Since $(\partial^2 p/\partial T^2)_\rho$ possesses small absolute values, except in the vicinity of the critical point, it is very difficult to measure accurately. To calculate C_v for compressed liquid states, additional data are required, including the vapor pressure and enthalpy of vaporization or heat capacity of the saturated liquid. Direct measurements of heat capacities provide useful checks on calculated heat capacities when they are available along a path traversing the temperature range of interest. In many cases, such data are scarce.

In a recent manuscript, Penoncello et al. [1] reviewed published thermodynamic property measurements for R23. Only four sources of heat capacity data for R23 were found. Just one of these contains saturated liquid heat capacities, and they cover a limited temperature range. Three of the sources presented heat capacities at constant pressure for gaseous samples. No liquid-phase heat capacities were found.

In this paper, heat capacity data are reported for the compressed gaseous region and both the single-phase and the saturated liquid region from near the triple-point temperature to the upper limit (345 K) of the apparatus. The triple-point temperature, enthalpy of fusion, and vapor pressures evaluated from two-phase heat capacity measurements are reported.

2. MEASUREMENTS

2.1. Apparatus and Procedures

The calorimeter used for these measurements has been described in detail by Goodwin [2] and Magee [3]. A spherical bomb contains a sample of known mass. The volume of the bomb, approximately 78 cm^3, is a function of temperature and pressure. A platinum resistance thermometer is attached to the bomb for the temperature measurement. Temperatures are reported on the ITS-90, after conversions from the original calibration on the IPTS-68. Pressures are measured with an oscillating quartz crystal pressure transducer with a 0- to 70-MPa range. Adiabatic conditions are ensured by a high vacuum (3×10^{-3} Pa) in the can surrounding the bomb,

by a temperature-controlled radiation shield, and by a temperature-controlled guard ring which thermally anchors the filling capillary and the lead wires to the bomb.

For the heat capacity measurement, a precisely determined electrical energy (Q) is applied and the resulting temperature rise ($\Delta T = T_2 - T_1$) is measured. We obtain the heat capacity from

$$C_v = \left(\frac{\partial U}{\partial T}\right)_v \cong \frac{Q - Q_0 - W_{pV}}{n\,\Delta T} \tag{2}$$

where U is the internal energy, Q_0 is the energy required to heat the empty calorimeter, W_{pV} is the change-of-volume work that results from the slight dilation of the bomb, and n is the number of moles enclosed in the bomb. In this work, the bomb was charged with sample up to the (p, T) conditions of the highest-density isochore. The bomb and its contents were cooled to a starting temperature in the single-phase region. Measurements were then performed in that region at increasing temperatures until either the upper temperature (345 K) or the pressure limit (35 MPa) was attained. For two filling densities, the bomb was then cooled to a temperature inside the two-phase region, and measurements were carried out on a two-phase sample. At the completion of a run, a small part of the sample was cryopumped into a lightweight cylinder for weighing. The next run was started at a lower density. All data points were measured from a single filling of the calorimetric bomb. After the last run was completed, the remaining sample was discharged and weighed.

A series of such runs with different fillings constitutes the investigation of the (p, T, C_v) surface. The ranges of temperature and pressure were predetermined to cover primarily the liquid-phase and compressed gaseous regions for R23. Within these ranges, C_v measurements were performed on 15 isochores for 111 state conditions at 127 to 342 K and 5.7 to 33.5 MPa. The two-phase heat capacity (leading to C_σ) measurements followed the path of (p, T) states defined by the vapor-pressure curves. For R23, 95 two-phase points were measured at temperatures from 121 to 295 K. A search of the literature disclosed the following. Four sources of heat capacity measurements at constant pressure (C_p) were found. No published C_v data were found. Grudzev and Shumskaya [4] reported C_p measurements at temperatures from 300 to 450 K and at pressures from 0.2 to 2 MPa. Rasskazov et al. [5] reported C_p measurements at temperatures from 250 to 370 K and at pressures from 0.5 to 5 MPa. Takanuma et al. [6] have reported C_p measurements at temperatures from 260 to 380 K and at pressures from 0.5 to 3 MPa. Finally, Valentine et al. [7] reported C_p measurements for R23 at temperatures from 122 to 190 K along the

saturated liquid curve. The Valentine et al. measurements will be useful for direct comparisons with this work.

2.2. Samples

High-purity samples were obtained for the measurements. The sample of R23 has a purity of 0.999999 mole fraction. Chemical analyses determined the impurities present, and their concentrations in parts per million (by volume) were as follows: air, 3; CO_2, 3; and, H_2O, 1. The acidity (as HCl) was determined to be 29 parts per billion (ppb) (by mass).

3. RESULTS

3.1. Heat Capacity

As mentioned in Section 2.1, adjustments should be applied to the raw heat-capacity data for the change-of-volume work of the bomb. During a measurement sequence, the volume of the bomb varies with the temperature and pressure in accordance with formulas reported previously [3]. It is an important adjustment since the bomb is thin-walled. Referring to Goodwin and Weber [8], we can obtain the work from

$$W_{pV} = \left(T_2 \left(\frac{\partial p}{\partial T} \right)_{V_2} - \frac{1}{2} \Delta p \right) \Delta V \tag{3}$$

where $\Delta p = p_2 - p_1$ is the pressure rise and $\Delta V = V_2 - V_1$ is the change of volume. The pressure derivative is calculated from an equation of state. Precise values for the pressure derivative were required, since this quantity can have a significant influence on the adjustment for the change-of-volume work. The first estimates of this derivative were calculated with an preliminary version of the fundamental equation of state reported by Penoncello et al. [9]. A closer examination of the behavior of the pressure derivative calculated with the preliminary equation showed unphysical behavior at densities higher than $1600\ \mathrm{kg \cdot m^{-3}}$ ($23\ \mathrm{mol \cdot L^{-1}}$). Since two densities in this work are higher than this amount, another preliminary equation of state (by Span and Lemmon [10]) was selected for further study. As a test, the C_v data for the seven isochores with the highest densities were processed with both equations of state [9, 10]. It became clear that the unphysical behavior at $\rho > 1600\ \mathrm{kg \cdot m^{-3}}$ was responsible for systematic errors of nearly 2% in C_v. Thus, the results at $\rho > 1600\ \mathrm{kg \cdot m^{-3}}$ calculated with the Span and Lemmon formulation were retained in the final table. A comparison of data at the next highest five densities showed

only negligible differences; thus, the data processed with the preliminary fundamental equation of Penoncello et al. were retained in the final table.

A minor adjustment is applied to the number of moles contained in the bomb. The total mass of the sample weighed is corrected by the amount residing in the noxious volume (combined internal volume of pressure transducer, charging valve, and tubing), which is approximately 0.2% of the bomb volume [3]. This amount is calculated from the noxious volume and densities obtained from an equation of state by using a quadratic temperature profile along the length of the capillary and pressure transducer.

Another minor adjustment is applicable only to the two-phase data. The number of moles residing in the noxious volume varies with the temperature and pressure of the sample in the bomb. In this volume, the substance is in the vapor state. Therefore, the raw heat capacity data must be corrected by the energy spent to evaporate the number of moles driven into the noxious volume during the heating interval [8].

The heat capacity data of each run are presented in Table I for two-phase states, and in Table II for single-phase states. The average of the initial and final temperatures of each heating interval is given for the data point temperature (ITS-90). In the single-phase liquid region, for each isochore, the tabulated pressures are calculated from a least-squares fit of the (p, T) data using a seven-term function $p = f(T)$, adopted from the equation of state of Jacobsen and Stewart [11]. In the two-phase region, however, most of the measured vapor pressures are below the accurate range of the pressure gauge (3 to 70 MPa). Thus, the pressures were calculated from a vapor-pressure equation [1] and are presented as calculated values in Table I. The density, given in Table II for single-phase states, is calculated from the corrected number of moles and the bomb volume. These experimental densities have an estimated uncertainty of 0.15% and could be used as supplementary information to define the thermodynamic properties of R32. In Table I, values of the two-phase heat capacity at constant volume ($C_v^{(2)}$) are presented as well as values of the saturated-liquid heat capacity C_σ [described by some authors as $C'_x = T(dS'/dT)$]. Values of C_σ are obtained by adjusting $C_v^{(2)}$ data with the equation given by Rowlinson [12],

$$C_\sigma = C_v^{(2)} - \frac{T}{\rho^2}\frac{d\rho_\sigma}{dT}\frac{dp_\sigma}{dT} + T\left(\frac{1}{\rho_\sigma} - \frac{1}{\rho}\right)\frac{d^2 p_\sigma}{dT^2} \tag{4}$$

where ρ_σ and p_σ are the density and pressure of the saturated liquid and ρ is the bulk density of the sample residing in the bomb. The derivative quantities were calculated with the ancillary equations of Penoncello et al. [1].

Table I. Two-Phase Heat Capacity $C_v^{(2)}$ and Heat Capacity of Saturated Liquid C_σ of R23

T_{avg} (K)	$\rho_{\sigma,avg}$ (mol · L^{-1})	$p_{\sigma,avg}$[a,b] (MPa)	$C_v^{(2)}$ (J · mol^{-1} · K^{-1})	C_σ (J · mol^{-1} · K^{-1})
120.6012	23.9166	0.0001	84.752	84.745
125.0614	23.7222	0.0002	84.312	84.300
129.4858	23.5261	0.0004	84.217	84.197
133.8703	23.3288	0.0007	84.103	84.071
138.2185	23.1304	0.0012	84.087	84.038
142.5308	22.9310	0.0019	84.002	83.931
146.8058	22.7310	0.0031	84.161	84.062
151.0343	22.5308	0.0048	83.928	83.794
155.2433	22.3292	0.0072	84.244	84.067
159.4146	22.1272	0.0105	84.403	84.176
163.5557	21.9244	0.0150	84.576	84.291
167.6643	21.7209	0.0209	84.927	84.577
171.7411	21.5167	0.0285	85.153	84.731
175.7796	21.3121	0.0382	85.421	84.922
179.7875	21.1066	0.0502	85.919	85.338
183.7601	20.9004	0.0650	86.423	85.759
187.7036	20.6930	0.0830	86.869	86.120
191.6161	20.4846	0.1045	87.293	86.460
195.5019	20.2747	0.1300	87.809	86.896
199.3516	20.0637	0.1598	88.473	87.486
203.1681	19.8513	0.1945	89.386	88.333
206.9596	19.6369	0.2344	90.108	89.000
210.7150	19.4208	0.2800	90.742	89.594
214.4421	19.2025	0.3316	91.198	90.030
218.1312	18.9822	0.3897	92.052	90.884
221.7941	18.7589	0.4547	92.789	91.648
225.4291	18.5326	0.5270	93.433	92.348
229.0344	18.3028	0.6070	94.290	93.299
232.6099	18.0693	0.6951	95.295	94.441
236.1588	17.8313	0.7916	96.131	95.464
239.6771	17.5886	0.8970	97.286	96.864
243.1680	17.3404	1.0115	98.133	98.025
246.6390	17.0855	1.1359	98.885	99.174
250.0674	16.8248	1.2697	99.903	100.683
253.4814	16.5551	1.4141	100.901	102.292
256.8607	16.2771	1.5688	102.213	104.356
260.2168	15.9886	1.7346	103.765	106.833
263.5495	15.6879	1.9118	104.746	108.956
266.8544	15.3738	2.1006	105.531	111.152
270.1301	15.0442	2.3011	106.836	114.213
122.9504	23.8146	0.0001	84.600	84.590
127.3893	23.6194	0.0003	84.297	84.281
131.7936	23.4226	0.0005	84.084	84.058
136.1634	23.2245	0.0009	83.867	83.827
140.4934	23.0255	0.0015	83.877	83.817
144.7892	22.8257	0.0025	83.864	83.779
153.2457	22.4251	0.0060	83.922	83.766
157.4309	22.2235	0.0088	84.281	84.078

Table I. *(Continued)*

T_{avg} (K)	$\rho_{\sigma,avg}$ (mol · L^{-1})	$p_{\sigma,avg}$ [a, b] (MPa)	$C_v^{(2)}$ (J · mol^{-1} · K^{-1})	C_σ (J · mol^{-1} · K^{-1})
161.5857	22.0211	0.0127	84.434	84.178
165.7065	21.8181	0.0179	84.617	84.298
169.7930	21.6146	0.0247	84.972	84.585
173.8498	21.4101	0.0333	85.322	84.860
177.8738	21.2050	0.0442	85.711	85.170
181.8615	20.9992	0.0576	86.301	85.677
185.8213	20.7923	0.0740	86.722	86.013
189.7509	20.5843	0.0937	87.055	86.262
193.6435	20.3755	0.1172	87.652	86.777
197.5054	20.1653	0.1449	88.394	87.442
201.3341	19.9538	0.1772	88.897	87.874
205.1318	19.7407	0.2145	89.635	88.552
208.8977	19.5258	0.2572	90.268	89.138
212.6369	19.3087	0.3058	90.766	89.605
216.3492	19.0891	0.3608	91.438	90.266
220.0255	18.8673	0.4223	92.370	91.212
223.6685	18.6428	0.4909	93.252	92.136
227.2861	18.4149	0.5671	94.011	92.970
230.8725	18.1835	0.6511	94.781	93.855
234.4263	17.9483	0.7433	95.880	95.115
237.9596	17.7080	0.8443	96.838	96.288
241.4604	17.4628	0.9542	97.668	97.396
244.9346	17.2118	1.0735	98.719	98.801
248.3844	16.9540	1.2026	99.717	100.242
251.8074	16.6887	1.3418	100.810	101.885
255.2008	16.4152	1.4913	102.087	103.841
258.5791	16.1310	1.6522	102.873	105.464
261.9293	15.8360	1.8241	104.155	107.778
265.2543	15.5280	2.0075	105.210	110.109
268.5435	15.2063	2.2022	107.030	113.506
265.1923	15.5339	2.0040	122.628	109.652
269.3848	15.1210	2.2542	126.184	113.819
273.5287	14.6796	2.5239	129.935	118.755
277.6144	14.2035	2.8130	133.476	124.342
281.6348	13.6825	3.1214	137.723	132.067
285.5785	13.0977	3.4486	143.539	144.070
289.4491	12.4047	3.7952	150.799	163.755
293.2072	11.5037	4.1577	159.927	202.991
267.2899	15.3311	2.1264	124.672	111.942
271.4707	14.9034	2.3871	128.163	116.306
275.5982	14.4442	2.6674	131.340	121.059
279.6566	13.9465	2.9666	135.849	128.241
283.6440	13.3959	3.2850	141.267	138.274
287.5645	12.7618	3.6232	147.162	152.848
291.3835	11.9817	3.9784	154.760	179.458
295.0715	10.8940	4.3477	167.026	241.192

[a] Subscript avg denotes a condition evaluated at the average of the initial and final temperatures.
[b] p_σ calculated from Ref. 9.

Table II. Heat Capacity C_v of Compressed Liquid and Gaseous R23

T_{avg} (K)	ρ_{avg} (mol · L^{-1})	p_{avg}[a] (MPa)	C_v (J · mol^{-1} · K^{-1})
127.0061	24.2029	20.1515	53.55
124.9802	24.2211	14.9677	53.86
129.0482	24.1853	25.2563	53.32
145.8102	23.3298	18.5519	51.67
149.9108	23.2985	27.3681	51.64
143.4026	23.3491	13.2547	52.22
147.5204	23.3166	22.2634	51.57
166.1617	22.3541	16.2386	50.74
170.3094	22.3263	23.8285	50.61
164.1146	22.3684	12.4665	51.09
168.2773	22.3398	20.1297	50.58
172.4125	22.3126	27.6187	50.75
186.4013	21.3635	14.7050	50.13
190.5803	21.3392	21.1612	50.19
194.7322	21.3158	27.4710	50.27
184.3193	21.3761	11.4902	50.59
188.5168	21.3511	17.9818	50.09
192.6959	21.3272	24.3911	50.15
196.8426	21.3040	30.6417	50.51
206.2878	20.3352	13.1924	50.20
210.5006	20.3142	18.6237	50.13
214.6893	20.2940	23.9696	50.45
218.8487	20.2742	29.2105	50.69
226.0154	19.2371	11.7767	50.68
230.2627	19.2191	16.2775	50.64
234.4929	19.2019	20.7405	50.90
238.6993	19.1850	25.1334	51.08
242.8655	19.1685	29.4451	51.21
246.4589	17.9853	10.6206	51.67
250.7651	17.9703	14.2523	51.48
255.0460	17.9559	17.8687	51.61
259.3145	17.9419	21.4587	51.75
263.5407	17.9281	24.9854	52.07
267.7615	17.9145	28.4787	52.40
271.9454	17.9010	31.9233	52.66
266.4777	16.5501	9.4803	52.84
270.8690	16.5376	12.3251	52.82
275.2448	16.5259	15.1682	52.74
279.6004	16.5145	17.9971	52.86
283.9401	16.5033	20.8087	53.32
288.2649	16.4923	23.6000	53.62
292.5594	16.4813	26.3602	53.84
296.8377	16.4704	29.0989	54.28

Table II. *(Continued)*

T_{avg} (K)	ρ_{avg} (mol · L^{-1})	p_{avg}[a] (MPa)	C_v (J · mol^{-1} · K^{-1})
301.1133	16.4596	31.8269	54.25
282.1566	14.7328	6.4766	55.05
286.6931	14.7191	8.5432	54.72
291.2173	14.7091	10.6230	54.39
295.7361	14.7000	12.7119	54.46
300.2487	14.6912	14.8046	54.57
304.7533	14.6826	16.8969	54.64
309.2484	14.6740	18.9857	54.64
313.7290	14.6655	21.0670	54.98
318.2098	14.6571	23.1465	55.23
322.6909	14.6487	25.2232	55.40
327.1644	14.6403	27.2926	55.65
331.6602	14.6318	29.3677	56.11
336.1689	14.6233	31.4431	56.49
340.7129	14.6148	33.5280	56.47
289.7340	14.0622	7.1848	55.79
294.4043	14.0508	9.0654	55.32
299.0838	14.0419	10.9668	55.12
303.7715	14.0335	12.8835	54.95
308.4535	14.0254	14.8057	54.95
313.1407	14.0174	16.7346	55.23
317.8329	14.0094	18.6678	55.15
322.5158	14.0014	20.5976	55.44
327.2102	13.9935	22.5313	55.73
331.9041	13.9856	24.4629	56.06
336.6037	13.9777	26.3944	56.25
341.3067	13.9698	28.3243	56.49
297.6856	13.1035	7.3991	57.04
302.4916	13.0938	9.0142	56.25
307.3258	13.0859	10.6563	56.09
312.1655	13.0785	12.3132	55.78
317.0186	13.0712	13.9840	55.88
321.8793	13.0641	15.6635	56.07
326.7482	13.0570	17.3497	55.84
331.6137	13.0500	19.0370	56.06
336.4836	13.0430	20.7271	56.08
341.3628	13.0359	22.4213	56.73
301.2179	11.5824	6.0742	59.81
306.1916	11.5735	7.3049	59.09
311.2022	11.5653	8.5659	58.17
316.2432	11.5586	9.8511	57.51
321.3083	11.5525	11.1554	57.51
326.3935	11.5465	12.4747	57.40

Table II. *(Continued)*

T_{avg} (K)	ρ_{avg} (mol · L^{-1})	p_{avg}[a] (MPa)	C_v (J · mol^{-1} · K^{-1})
331.5024	11.5407	13.8075	57.16
336.6187	11.5348	15.1477	56.97
341.7584	11.5290	16.4979	57.14
306.2018	11.5735	7.3075	59.01
311.2360	11.5653	8.5745	58.21
316.2876	11.5586	9.8625	57.43
321.3697	11.5524	11.1713	57.33
326.4738	11.5465	12.4956	57.40
331.5958	11.5406	13.8320	57.44
336.7304	11.5347	15.1770	57.10
341.8805	11.5289	16.5300	56.99
305.9120	8.0973	5.6952	69.34
311.3572	8.0925	6.4186	64.98
316.9101	8.0869	7.1657	62.98
322.5377	8.0815	7.9294	61.30
328.2127	8.0767	8.7040	60.18
333.9414	8.0725	9.4892	60.04
339.7095	8.0686	10.2821	59.18
305.8892	8.0974	5.6922	69.62
311.3319	8.0925	6.4152	64.98
316.8740	8.0869	7.1608	62.61
322.4851	8.0815	7.9222	61.42
328.1678	8.0768	8.6979	60.58
333.8880	8.0726	9.4818	59.82
339.6369	8.0686	10.2721	59.15

[a] Subscript avg denotes a condition evaluated at the average of the initial and final temperatures.

The saturated-liquid heat capacity C_σ, as a saturation quantity, depends only on temperature. If the data are internally consistent, then the values at saturation measured at different filling densities should fall on a single curve. Although the C_σ values were evaluated from experiments with two widely different amounts of sample in the calorimeter, the results should demonstrate consistency of all isochores.

The saturated liquid heat capacities for all of the filling densities are depicted graphically in Fig. 1. In order to intercompare the data from the two densities, an equation which accurately describes the whole two-phase data set was derived. For R23, the expression,

$$C_\sigma/C_0 = b_1\tau^{-0.94} + b_2\tau^{-0.13} + b_3\tau^{4.3} \tag{5}$$

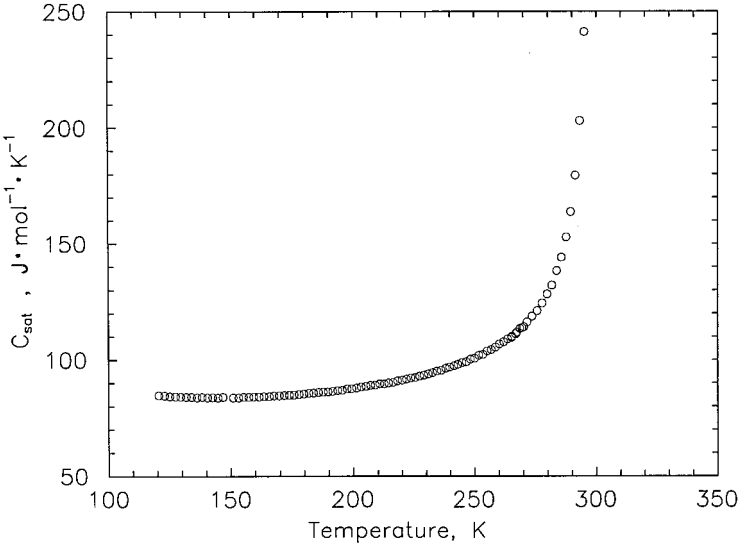

Fig. 1. Experimental saturated-liquid heat capacity (C_σ) values for R23.

where $C_0 = 1\ \mathrm{J \cdot mol^{-1} \cdot K^{-1}}$, $\tau = 1 - T/T_c$, $T_c = 299.30$ K, $b_1 = 2.19$, $b_2 = 70.23$, and $b_3 = 55.35$, was fitted to the data. Equation (5) is valid at temperatures from 120 to 295 K along the saturated liquid curve. The deviations are shown in Fig. 2. Deviations are distributed randomly over the entire temperature range. The heat capacities at saturation for the two filling densities agree within the uncertainty of the measurements, indicating that there is good internal consistency within the data set. The approximation $C_{p,\sigma} \cong C_v^{(2)} \cong C_\sigma$, valid at low pressures on the saturated liquid curve, makes it possible to compare the $C_{p,\sigma}$ of Valentine et al. with Eq. (5). The deviations plotted in Fig. 2 show that the Valentine et al. data deviate systematically by about -0.3% from this work. Since this amount is smaller than the uncertainty we have reported for our C_σ data, this agreement is very good.

Values of the single-phase liquid heat capacity are shown in Fig. 3. The data are presented on isochores in a C_v–T diagram. Most liquid isochores overlap in their temperature ranges, except at the highest densities, where C_v is observed to increase. There is a visible critical enhancement in the C_v values near the critical-density isochore.

When this document was prepared, the only other published heat capacity data for R23 were the four sets of isobaric heat capacity (C_p) data mentioned earlier. Although most of the published data are of high accuracy, those values were not used in the development of the equation

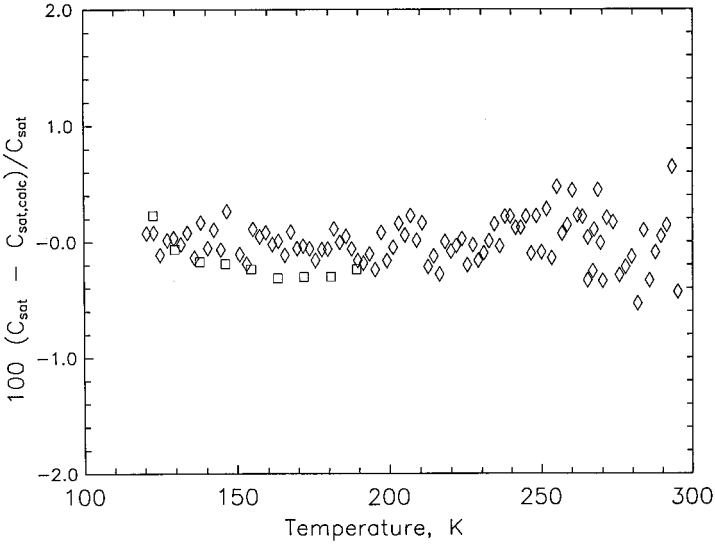

Fig. 2. Comparison of experimental C_σ results for R23 with values calculated with Eq. (5): ◇, this work; □, Valentine et al. [7].

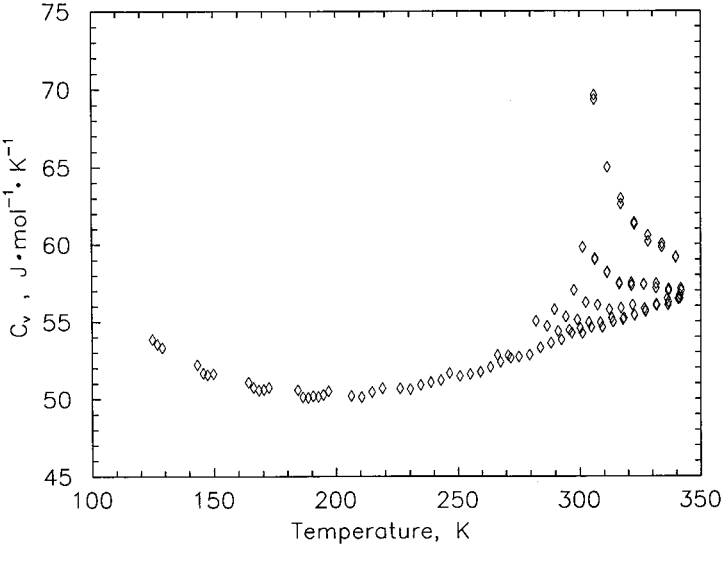

Fig. 3. Experimental compressed liquid and gaseous heat capacity (C_v) data for R23.

of state of Penoncello et al. [1]. Since the present results were used by Penoncello et al., their equation of state will facilitate an indirect comparison with published data. Table 11 in Ref. 1 shows comparisons of C_v and C_p with the equation of state of Penoncello et al. The absolute average deviation (AAD) for the C_v data from this work is 0.51%, with a bias of −0.20%. The AAD for the C_p data of Gruzdev and Shunskaya is 0.92%, with a bias of −0.92%. The AAD for the C_p data of Rasskazov et al. is 2.57%, with a bias of −2.57%. The AAD for the C_p data of Takanuma et al. is 4.10%, with a bias of −4.05%. The AAD for the C_p data of Valentine et al. is 0.58%, with a bias of −0.20%. This work is in very good agreement with published heat capacities for R23. In a wide temperature range between the triple point (118 K) and 243 K, there are no published liquid-phase heat capacity data. Taken as a whole, most of the calculated values of C_v are within ±1% of the measurements and most of the C_p values are within ±2%.

3.2. Derived Vapor Pressures

At temperatures well below the normal boiling point, vapor pressures measured with traditional techniques are often inaccurate. In some cases, volatile impurities concentrate in the vapor phase [13] as temperature is decreased. This will influence the vapor pressure measurement, making it appear larger than the true value for the pure substance. Another common problem is that pressure gauges are not accurate enough under such low pressure conditions. This situation can be remedied to some extent, however, by extracting vapor pressure values from two-phase heat capacity measurements. We have shown that $C_v^{(2)}$ values have an excellent internal consistency and have their lowest uncertainty below the normal boiling point because the necessary adjustments to the $C_v^{(2)}$ measurements for vaporization and pV work are less than 0.1% of the resulting $C_v^{(2)}$ value. We elected to use this method [14] to calculate vapor pressures from the data in Table I.

In the present work, only a brief summary is given for the technique to calculate vapor pressures from isochoric internal-energy measurements in the two-phase region. A detailed discussion is presented in the original work [14]. The method is based on the expression relating the two-phase internal energy $U^{(2)}$ to the vapor pressure,

$$(\partial U^{(2)}/\partial V)_T = T\left(\frac{dp}{dT}\right)_\sigma - p_\sigma = T^2\left(\frac{d(p/T)}{dT}\right)_\sigma \tag{6}$$

where σ signifies a quantity evaluated on the liquid–vapor saturation boundary. By exploiting the linear dependence of $U^{(2)}$ on the molar volume V,

the derivative on the left side of Eq. (6) can be replaced with a finite difference calculation,

$$(\partial U^{(2)}/\partial V^{(2)})_T = \left(\frac{U_2^{(2)} - U_1^{(2)}}{V_2^{(2)} - V_1^{(2)}}\right)_T \tag{7}$$

where subscripts 1 and 2 denote any two points within the two-phase region, including the points at the saturated single phases, and the superscript (2) denotes the bulk property. In this work, a bulk property is any property of the vapor and the liquid combined.

After computing $(\partial U^{(2)}/\partial V^{(2)})_T$ at different temperatures between the triple point and the normal boiling point, we can fit Eq. (6) to these data using a nonlinear regression analysis [15] of the parameters in an equation for $p_\sigma(T)$. As indicated by Eq. (6), the regression analysis must fit the adjustable parameters in the difference between two equations given by $T(dp/dT)_\sigma - p_\sigma$. This is the reason why it is important to select an equation $p_\sigma = f(T)$ which is capable of fitting vapor pressure data within their experimental uncertainty over the entire temperature range of interest. Experience has indicated which $p_\sigma(T)$ equations [14] have desirable properties.

Experimental values for $U^{(2)}$ at precisely known densities are required to carry out the calculations with Eq. (7). We will use experimental energy-increment data from isochoric (constant-$V^{(2)}$) measurements which were measured in this work. Values for $U^{(2)}$ at two or more densities are needed to calculate the change of the bulk internal energy with respect to the bulk specific volume at constant temperature. Since the calorimetric measurements provide the change of internal energy as a function of T along a given isochore, but not the change of internal energy from one density to another, we need additional information at a reference temperature to determine the change of internal energy between two densities. This reference temperature is selected near the normal boiling point, where accurate, direct measurements of the vapor pressure are available.

The value of $(\partial U^{(2)}/\partial V^{(2)})_T$ at the reference temperature can be calculated with Eq. (6) and vapor pressure data around the reference temperature. Then, the change of internal energy from density 1 to density 2 at that reference temperature can be determined from

$$U_2^{(2)} - U_1^{(2)} = (\partial U^{(2)}/\partial V^{(2)})_T (V_2^{(2)} - V_1^{(2)}) \tag{8}$$

In this procedure, we set the internal energy of one of the densities ($U_2^{(2)}$ or $U_1^{(2)}$) to an arbitrary value $U_i^{(2)} = 0$ at the reference temperature. Then internal energy increments are calculated at each temperature and density based on differences in U from this reference state.

Penoncello et al. [1] has shown the existence of systematic discrepancies of about $\pm 1\%$ among the four sources of reliable published vapor pressure data for R23 in the temperature range 133 to 200 K. In fact, three data sources give three distinctly shaped, nonoverlapping curves which are observed to fan out at temperatures below the normal boiling point. In addition to this concern, at temperatures $T < 141$ K there is just one source of data, and at $T < 133$ K there is none. Our goal is to use the $U^{(2)}$ measurements in this work to calculate vapor pressures to compare with published data and to extend the range of available vapor pressures. The normal boiling-point temperature of R23 is about 191.09 K [16] and the triple point is 118.02 K. A temperature of 190 K was selected for the reference temperature due to the availability of tabulated saturation data. The internal-energy reference state, where we arbitrarily set $U^{(2)} = 0$, was selected as the saturated vapor state at 190 K. We will calculate vapor pressures for R23 from 190 K to the triple-point temperature. These calculations will give us thermodynamically consistent vapor pressures up to about 0.1 MPa which can be used to validate direct measurements.

To apply Eq. (7), we need internal energies for both a high-density state and a low-density state, both at the same temperature. For the low-density states, we used internal energies of the saturated vapor from the Span and Lemmon equation of state [10]. Each of these states was paired with a high-density state from calorimetric measurements. The difference in internal energy between these two curves is about $15\ \mathrm{kJ \cdot mol^{-1}}$ at the reference temperature and about $20\ \mathrm{kJ \cdot mol^{-1}}$ at the triple-point temperature. The large absolute values we obtained for $\Delta U^{(2)}$ lead to reliable values of $(\partial U^{(2)}/\partial V^{(2)})_T$ and to accurate vapor pressures.

We selected a vapor pressure equation of the same functional form used for R152a [17],

$$\ln(p_\sigma/p_c) = [C_1\tau + C_2\tau^{1.5} + C_3\tau^2 + C_4\tau^4 + C_5\tau^{6.5}]/[1-\tau] \qquad (9)$$

where $\tau = 1 - T/T_c$, $T_c = 299.30$ [10] K, and $p = 4.83$ MPa [10] for R23.

In this analysis, the change in internal energy along the high density isochore was determined from two-phase calorimetric data reported in this work. We chose an isochore that includes measurements from 120.6 to 200 K. For this isochore, the calorimetric bomb (with a volume of approximately $78\ \mathrm{cm^3}$) contained 1.1453 mol of sample. The energy needed to change the temperature of the sample by 1 K was fitted with the equation

$$Q/(n\,\Delta T) = a_0 + a_1 T^{-1} + a_2 T^{-2} \qquad (10)$$

where Q is in J, n is in mol, and T is in K. The coefficients are $a_0 = 1.32193502 \times 10^2$, $a_1 = -1.35749740 \times 10^4$, and $a_2 = 9.51389556 \times 10^5$.

Table III. Vapor Pressures of R23 Derived from $U^{(2)}$ Measurements

T (K)	$p_{\sigma,\,\mathrm{pub}}$[a] (Pa)	$p_{\sigma,\,\mathrm{this\ work}}$[b] (Pa)	Dev.[c] (Pa)
190.000	94,908.0	94,859.3	48.7
189.000	89,477.8	89,428.9	48.9
188.000	84,298.0	84,248.1	49.9
187.000	79,360.4	79,308.7	51.7
186.000	74,656.7	74,602.7	54.0
185.000	70,178.8	70,122.1	56.7
184.000	65,918.8	65,859.0	59.8
183.000	61,868.9	61,805.8	63.2
182.000	58,021.5	57,954.9	66.6
181.000	54,369.1	54,298.9	70.1
180.000	50,904.3	50,830.7	73.6
179.000	47,620.0	47,543.1	77.0
178.000	44,509.2	44,429.1	80.1
177.000	41,565.0	41,482.0	83.0
176.000	38,780.7	38,695.1	85.6
175.000	36,149.7	36,061.9	87.9
174.000	33,665.7	33,576.0	89.7
173.000	31,322.5	31,231.3	91.1
172.000	29,113.9	29,021.8	92.1
171.000	27,034.1	26,941.5	92.6
170.000	25,077.3	24,984.6	92.7
169.000	23,238.0	23,145.7	92.3
168.000	21,510.7	21,419.3	91.4
167.000	19,890.2	19,800.1	90.1
166.000	18,371.3	18,283.0	88.3
165.000	16,949.2	16,863.0	86.2
164.000	15,619.0	15,535.3	83.7
163.000	14,376.1	14,295.3	80.8
162.000	13,216.0	13,138.4	77.6
161.000	12,134.5	12,060.3	74.1
160.000	11,127.2	11,056.8	70.4
159.000	10,190.3	10,123.8	66.5
158.000	9,319.8	9,257.4	62.4
157.000	8,512.1	8,453.9	58.2
156.000	7,763.4	7,709.6	53.9
155.000	7,070.5	7,021.0	49.5
154.000	6,429.9	6,384.8	45.1
153.000	5,838.6	5,797.8	40.8
152.000	5,293.5	5,257.0	36.5

Table III. *(Continued)*

T (K)	$p_{\sigma,\,\mathrm{pub}}$[a] (Pa)	$p_{\sigma,\,\mathrm{this\ work}}$[b] (Pa)	Dev.[c] (Pa)
151.000	4,791.6	4,759.4	32.2
150.000	4,330.3	4,302.2	28.1
149.000	3,906.9	3,882.8	24.1
148.000	3,518.9	3,498.5	20.3
147.000	3,163.8	3,147.1	16.7
146.000	2,839.5	2,826.2	13.2
145.000	2,543.7	2,533.6	10.0
144.000	2,274.3	2,267.3	7.0
143.000	2,029.6	2,025.3	4.2
142.000	1,807.5	1,805.8	1.7
141.000	1,606.5	1,607.1	−0.6
140.000	1,424.8	1,427.4	−2.6
139.000	1,260.9	1,265.3	−4.5
138.000	1,113.3	1,119.3	−6.0
137.000	980.8	988.2	−7.4
136.000	862.0	870.5	−8.5
135.000	755.7	765.2	−9.5
134.000	660.9	671.1	−10.2
133.000	576.5	587.3	−10.7
132.000	501.6	512.7	−11.1
131.000	435.2	446.5	−11.3
130.000	376.5	387.9	−11.4
129.000	324.8	336.2	−11.4
128.000	279.4	290.6	−11.2
127.000	239.6	250.5	−10.9
126.000	204.8	215.4	−10.6
125.000	174.5	184.6	−10.2
124.000	148.1	157.9	−9.7
123.000	125.4	134.6	−9.2
122.000	105.7	114.4	−8.7
121.000	88.8	96.9	−8.1
120.000	74.3	81.8	−7.5
119.000	61.9	68.9	−7.0
118.000	51.4	57.8	−6.4
118.020	51.6	58.0	−6.4

[a] Equation (9) fitted to data from Popowicz *et al.* [18].
[b] Equation (9) fitted to data from $U^{(2)}$ increments.
[c] Dev. $= p_{\sigma,\,\mathrm{Popowicz}} - p_{\sigma,\,U^{(2)}}$.

The change of internal energy along the isochore is then calculated with

$$\Delta U = \int_{T_1}^{T_2} Q/(n\,\Delta T)\,dT \tag{11}$$

where $n = 1.1453$ mol.

Although the exact bomb volume varies with temperature and pressure, we may approximate the density as a function of temperature only. The density of the *quasi-isochore* was fitted with the equation

$$\rho = b_0 + b_1 T^{-1} + b_2 T^{-2} \tag{12}$$

where ρ is in $\text{mol} \cdot \text{dm}^{-3}$ and the coefficients are $b_0 = 6.06634949$, $b_1 = 3.83067299 \times 10^3$, and $b_2 = -2.02949652 \times 10^5$. The molar mass used for R23 is $70.014\ \text{g} \cdot \text{mol}^{-1}$ [16].

The internal energy of the saturated vapor was calculated from $U = H - PV$ with values of U calculated with the equation of state by Span and Lemmon [10]. Sensitivity studies [14] have shown that the results are insensitive to the choice of a gas-phase equation of state as long as it reproduces the correct behavior of the second virial coefficients. A value of $(\partial U^{(2)}/\partial V^{(2)})_T$ at the reference temperature (190 K) was calculated with the vapor-pressure ancillary equation, Eq. (9), fitted to the published vapor pressures of Popowicz et al. [18]; vapor pressures calculated in this way are shown in the second column in Table III. After application of this method to calculate vapor pressures from internal energy increments, the final vapor pressure coefficients in Eq. (9) are $C_1 = -7.32026743$, $C_2 = 1.72415498$, $C_3 = -1.04915426$, $C_4 = -3.52955949$, and $C_5 = 0.347525072$. Table III presents the vapor pressures calculated from internal energy increments in the third column, and the fourth column gives the deviation of p_σ values calculated with a fit to the Popowicz et al. measurements from the new results. Figure 4 depicts the deviations of our equation fit to Popowicz et al. data from Eq. (9). The agreement shown with Popowicz et al. is very good. At a temperature 15 K above the triple-point temperature (133 K), the deviation, defined as the difference between an experimental point and a calculated value, is just -11 Pa (-2%), at 160 K it is 70 Pa (0.6%), and at 190 K it is 49 Pa (0.05%).

3.3. Triple Points

The triple-point temperature (ITS-90) of R23 was measured in three experiments. The sample was slowly cooled to a temperature about 2 K

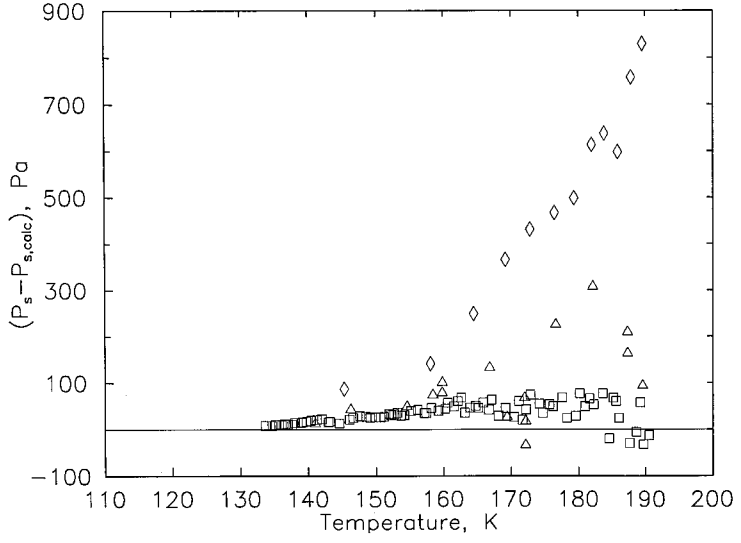

Fig. 4. Comparison of published vapor pressures with values calculated with Eq. (9): zero line, this work, calculated from $U^{(2)}$ increments; □, Popowicz et al. [18]; △, Hou and Martin [19]; ◇, Valentine et al. [7].

below freezing. The solidified sample was then heated at a constant power of 0.09 W. To obtain a slowly increasing temperature, heater power was set to a value which is less than one-tenth of the power for heat capacity experiments. Data were evaluated graphically. The triple point was located by noting a sharp break in the rate of temperature rise, delineating when melting began. Each experiment lasted about 970 min (16 h). The results and their expanded uncertainties for T_{tr} of the three samples were 118.025 ± 0.02, 118.025 ± 0.02, and 118.023 ± 0.02 K. Thus, the average of 118.02 ± 0.02 K was adopted for T_{tr} of R23. This value is 0.047 K above the only published measurement [7], 117.973 K, which is within the combined uncertainties. The enthalpy of fusion $\Delta_{fus}H$ was measured by integrating the applied heater power over the time of heating and applying a correction for parasitic heat losses. The results and expanded uncertainties for $\Delta_{fus}H$ obtained from the three runs were 4128 ± 30, 4107 ± 30, and 4124 ± 30 J · mol^{-1}; the average of 4120 ± 30 J · mol^{-1} is the best estimate for $\Delta_{fus}H$ at the triple point.

3.4. Assessment of Uncertainties

Uncertainty in C_v arises from several sources. Primarily, the accuracy of this method is limited by the uncertainty of the temperature rise

measurement and the change-of-volume work adjustment. In the following discussion, the definition for the expanded uncertainty, which is two times the standard uncertainty, corresponds to a coverage factor $k = 2$ and thus a two-standard deviation estimate.

Different sources of uncertainty, including calibration of the platinum resistance thermometer, radiation to or from the thermometer head, and drift of the ice-point resistance, contribute to an expanded uncertainty of 0.01 K (at 100 K) to 0.03 K (at 345 K) for the absolute temperature measurement. The uncertainty of the temperature rise also depends on the reproducibility of temperature measurements. The temperatures assigned to the beginning (T_1) and to the end (T_2) of a heating interval are determined by extrapolation of a linear temperature drift (approximately -1×10^{-3} to 0.5×10^{-3} K · min^{-1}) to the midpoint time of the interval. This procedure leads to an uncertainty of 0.001 to 0.004 K for the extrapolated temperatures T_1 and T_2, depending on the standard deviation of the linear function correlated. In all cases, values from 0.002 to 0.006 K were obtained for the uncertainty of the temperature rise, $\Delta T = T_2 - T_1$. For a typical experimental value of $\Delta T = 4$ K, this corresponds to a relative uncertainty of between 0.05 and 0.15%.

The uncertainty of the change-of-volume work influences primarily the single-phase values, since two-phase experiments are performed over a small pressure interval. The ratio of change-of-volume work to total applied heat may be as large as 0.11 for the highest-density isochore down to 0.005 for the lowest density. Estimated uncertainties of 2.3 to 3.0% in the change-of-volume work are due to both the deviation of the calculated pressure derivatives and the uncertainty of the volume change. This leads to a relative uncertainty of 0.2% in C_v for the lowest-density isochore up to 0.3% for the highest density.

The energy applied to the calorimeter is the integral of the product of voltage and current from the initial to the final heating time. Voltage and current are measured 20 times during a heating interval. The measurements of the electrical quantities have a relative uncertainty of 0.01%. However, we must account for the effect of radiation heat losses or gains which occur when a time-dependent lag of the controller leads to a small temperature difference of about 20 mK between the bomb and the radiation shield at the beginning and end of a heating period. Since heat transfer by radiation is proportional to $T_1^4 - T_2^4 \approx 4T^3 \Delta T$, we would expect radiation losses to increase substantially with the bomb temperature. Therefore, the relative uncertainty in the applied heat is estimated to be 0.02% for lower temperatures and up to 0.10% for the highest temperatures. This leads to a relative uncertainty in C_v between 0.04 and 0.20%.

The energy applied to the empty calorimeter has been measured in repeated experiments and fitted to a function of temperature [3]; its relative uncertainty is less than 0.02%. Its influence on the uncertainty of the heat capacity is reduced because the ratio of the heat applied to the empty calorimeter to the total heat varies only from 0.35 to 0.70 for the single-phase runs and from 0.61 to 0.62 for the two-phase runs. The mass of each sample was determined with a relative uncertainty of 0.01% by differential weighings before and after trapping the sample. The density calculated from this mass and the bomb volume has a relative uncertainty of approximately 0.2%. For pressures, the uncertainty of the gauge of 7 kPa is added to the cross term for the pressure derivative in the change-of-volume work adjustment. However, neither the uncertainty of p nor ρ contributes appreciably to the combined uncertainty for molar heat capacity. We may combine the various sources of experimental uncertainty using a root-sum-of-squares formula. The relative uncertainty is estimated to be 0.7% for C_v, 0.5% for $C_v^{(2)}$, and 0.7% for C_σ.

4. CONCLUSIONS

For R23, 111 single-phase heat capacities, 94 saturated-liquid heat capacities, 73 derived vapor pressures, and values for the temperature and enthalpy of fusion at the triple point were reported. Agreement with a published value of the triple-point temperature was within 0.047 K. Published liquid-phase heat capacity data are scarce and cover limited ranges of temperature and pressure. Agreement with published saturated-liquid heat capacity values at constant pressure was within 0.3%.

ACKNOWLEDGMENTS

The authors are grateful to Mark McLinden, Eric Lemmon, and Roland Span for generous technical assistance and helpful discussions during this study. We have profited from many discussions with Torsten Lüddecke, Mickey Haynes, and Marcia Huber.

REFERENCES

1. S. G. Penoncello, Z. Shan, and R. T Jacobsen, *ASHRAE Trans.* **106**:739 (2000).
2. R. D. Goodwin, *J. Res. Natl. Bur. Stand. (U.S.)* **65C**:231 (1961).
3. J. W. Magee, *J. Res. Natl. Inst. Stand. Technol.* **96**:725 (1991).
4. V. A. Gruzdev and A. I. Shumskaya, in *Thermophysical Properties of Matter and Substances, Vol. 8*, V. A. Rabinovich, ed. (GS SSD, Moscow, 1975), pp. 108–129 (in Russian).

5. D. S. Rasskazov, G. A. Spiridonov, and L. A. Krewkov, in *Thermophysical Properties of Matter and Substances*, *Vol. 8*, V. A. Rabinovich, ed. (GS SSD, Moscow, 1975), pp. 100–107 (in Russian).
6. A. Takanuma, M. Uematsu, and K. Watanabe, *Nippon Reito Kyokai Ronbunshu*, *Vol. 2* (1985).
7. R. H. Valentine, G. E. Brodale, and W. F. Giauque, *J. Phys. Chem.* **66**:392 (1962).
8. R. D. Goodwin and L. A. Weber, *J. Res. Natl. Bur. Stand. (U.S.)* **73A**:1 (1969).
9. S. G. Penoncello, personal communication (University of Idaho, Moscow, 1999).
10. R. Span and E. W. Lemmon, personal communication (Ruhr University Bochum, Bochum, Germany, 1999).
11. R. T Jacobsen and R. B. Stewart, *J. Phys. Chem. Ref. Data* **2**:757 (1973).
12. J. S. Rowlinson, *Liquids and Liquid Mixtures* (Butterworths, London, 1969), p. 37.
13. L. A. Weber, *Int. J. Refrig.* **17**:117 (1992).
14. H. A. Duarte-Garza and J. W. Magee, *Int. J. Thermophys.* **18**:173 (1997).
15. P. T. Boggs, R. H. Byrd, J. E. Rogers, and R. B. Schnabel, *NISTIR 4834*, *User's Reference Guide for ODRPACK Version 2.01*, *Software for Weighted Orthogonal Distance Regression* (NIST, Gaithersburg, MD, 1992).
16. M. O. McLinden, M. L. Huber, and S. L. Outcalt, *Proceedings*, *ASME Winter Annual Meeting*, New Orleans, No. 93-WA/HT-29 (ASME, New York, 1993).
17. H. A. Duarte-Garza and J. W. Magee, *Int. J. Thermophys.* **20**:1467 (1999).
18. A. Popowicz, T. Oi, J. Shulman, and T. Ishida, *J. Chem. Phys.* **76**:3732 (1982).
19. Y. C. Hou and J. J. Martin, *AIChE J.* **5**:125 (1959).